J Neurophysiol 107: 2352–2365, 2012.
First published February 1, 2012; doi:10.1152/jn.00852.2011.

The representations of reach endpoints in posterior parietal cortex depend on which hand does the reaching

Steve W. C. Chang and Lawrence H. Snyder
Department of Anatomy and Neurobiology, Washington University in St. Louis School of Medicine, St. Louis, Missouri

Submitted 19 September 2011; accepted in final form 31 January 2012

Chang SWC, Snyder LH. The representations of reach endpoints in posterior parietal cortex depend on which hand does the reaching. *J Neurophysiol* 107: 2352–2365, 2012. First published February 1, 2012; doi:10.1152/jn.00852.2011.—Neurons in the parietal reach region (PRR) have been implicated in the sensory-to-motor transformation required for reaching toward visually defined targets. The neurons in each cortical hemisphere might be specifically involved in planning movements of just one limb, or the PRR might code reach endpoints generically, independent of which limb will actually move. Previous work has shown that the preferred directions of PRR neurons are similar for right and left limb movements but that the amplitude of modulation may vary greatly. We now test the hypothesis that frames of reference and eye and hand gain field modulations will, like preferred directions, be independent of which hand moves. This was not the case. Many neurons show clear differences in both the frame of reference as well as in direction and strength of gain field modulations, depending on which hand is used to reach. The results suggest that the information that is conveyed from the PRR to areas closer to the motor output (the readout from the PRR) is different for each limb and that individual PRR neurons contribute either to controlling the contralateral-limb or else bimanual-limb control.

contralateral- and ipsilateral-limb specificity; parietal reach region; reference frame; sensorimotor transformation

ACTION PLANNING REQUIRES THE selection of a particular motor effector. This selection ultimately determines which muscles will be activated and therefore, determines the relevant frame of reference for the movement. For instance, the direction of a reach to a target along the body midline may differ by 180° depending on the hand that is selected to perform the action. It is not surprising then that effector selection has pronounced effects on spatially tuned responses in premotor and posterior parietal neurons (Caminiti et al. 1991; Chang et al. 2008; Cisek et al. 2003; Crawford et al. 2004; Hoshi and Tanji 2000; Kalaska et al. 1997; Kermadi et al. 2000; Medendorp et al. 2005). Some neurons are active only for planned contralateral hand movements, others only for planned ipsilateral movements, and still others for movements of either hand (Chang et al. 2008; Cisek et al. 2003; Hoshi and Tanji 2006; Kermadi et al. 2000; Medendorp et al. 2005).

The reference frame in which neurons encode spatial information is fundamental to understanding spatial processing, sensorimotor transformations across multiple modalities, and eye-hand coordination (Andersen et al. 1997; Burnod et al. 1992; Colby 1998; Crawford et al. 2004; Flanders et al. 1992; Kalaska et al. 1997; McIntyre et al. 1997). Neurons in the striate cortex and extrastriate visual areas encode visual stimuli with respect to the point of visual regard, that is, in a retinocentric or gaze-centered frame of reference (Connor et al. 1996; Felleman and Van Essen 1987; Maunsell and Van Essen 1983). In contrast, neurons in the primary motor cortex (M1) and spinal cord often use muscle- or joint-centered reference frames (Caminiti et al. 1991; Crawford et al. 2004; Kakei et al. 1999; Kalaska et al. 1997; Scott and Kalaska 1995, 1997). Experimental studies suggest that neurons in the intervening areas (neither purely sensory nor purely motor) encode spatial information using diverse reference frames that are often idiosyncratic to each neuron (Batista et al. 2007; Chang and Snyder 2010; Fetsch et al. 2007; Jay and Sparks 1987; McGuire and Sabes 2011; Mullette-Gillman et al. 2005; Pesaran et al. 2006; Stricanne et al. 1996). For example, neurons in the parietal reach region (PRR) and dorsal premotor cortex (PMd) use a range of gaze-centered, hand-centered, and intermediate representations to specify the targets for upcoming visually guided reaches (Batista et al. 2007; Chang and Snyder 2010; Marzocchi et al. 2008; Pesaran et al. 2006). Computational studies have demonstrated that using a range of reference frames may introduce helpful complexity, allowing a brain area to serve multiple objectives (Avillac et al. 2005; Blohm et al. 2009; McGuire and Sabes 2009; Pouget and Snyder 2000; Xing and Andersen 2000). Thus cortical neurons show both a range of reference frames as well as a range of effector specificities. It is not known, however, whether these properties sort independently or are in some way linked.

The PRR (Galletti et al. 1997; Snyder et al. 1997) is located in the posterior parietal cortex (PPC), a cortex that links sensation with action (Colby 1998; Goodale and Milner 1992). The PRR straddles the boundary between the medial intraparietal area (MIP) and V6A (Calton et al. 2002; Chang et al. 2008; Snyder et al. 1997). PRR neurons discharge while planning an upcoming reach to a visual and auditory target and have been implicated in sensorimotor transformations for reaching (Batista et al. 1999; Battaglia-Mayer et al. 2001; Chang et al. 2009; Cohen and Andersen 2000; Fattori et al. 2001; Galletti et al. 1997; Snyder et al. 1997). However, whether the PRR mediates limb-specific or limb-nonspecific transformations remains unknown.

Our previous study showed that the preferred directions of PRR neurons are similar for reaches with the contralateral and ipsilateral hand, whereas the magnitude of modulation can differ drastically (Chang et al. 2008). It remains unknown what happens to the frame of reference when animals reach with one or the other hand. To determine this, it is necessary to record responses to reaches with either hand using different starting eye and hand positions (Mullette-Gillman et al. 2009). Arguably, a single frame would be particularly useful if the PRR

Address for reprint requests and other correspondence: S. W. C. Chang, Center for Cognitive Neuroscience, Dept. of Neurobiology, Duke Univ. Medical Center, Durham, NC 27701 (e-mail: steve@eye-hand.wustl.edu).

controls movements of either limb. In fact, this was one virtue of the gaze-based frame of reference that was originally associated with the PRR (Batista et al. 1999; Cohen and Andersen 2000). If the PRR instead affects movements of only one limb, then having matching reference frames across the two limbs is of little consequence.

Here, we test the hypothesis that reference frames of individual neurons will be similar regardless of which hand is used to reach. Based on our results, we reject this hypothesis. We also found that gain field modulations depend on which limb is being used. Thus when one compares coding in the PRR for movements of the contralateral vs. ipsilateral limb, there are not only differences in overall responsiveness (Chang et al. 2008) but also in the frame of reference and in gain field modulations.

METHODS

Behavior. All procedures conformed to the Guide for the Care and Use of Laboratory Animals and were approved by the Washington University Institutional Animal Care and Use Committee. Two male rhesus macaques (*Macaca mulatta*) participated in the study. Eye position was monitored by the scleral search coil technique (CNC Engineering, Seattle, WA). Hand position was monitored by a 13.2 × 13.2-cm custom-built touch panel that uses finely spaced (3 mm) horizontal and vertical infrared beams, 1–3 mm above a smooth touch surface (2 ms temporal resolution). Touching the surface resulted in breaking one or more beams, typically with the index finger or the index and middle fingers together. The animals sat in a custom-designed monkey chair (Crist Instrument, Hagerstown, MD) with a fully open front to allow unimpaired reaching movements. Visual stimuli were back projected by a cathode ray tube projector onto the touch surface, which was mounted vertically, 25 cm in front of the animal. The recording room was sound attenuating and light proof, such that a dark-adapted human could detect no light when the projector was turned on but projecting no targets.

In the preferred direction mapping task, animals made center-out reaching arm movements while maintaining central fixation. Animals first fixated and pointed at a blue center target (2.4° × 2.4° within a 4° radius). A peripheral target (2.4° × 2.4°) appeared at one of 16 locations at 12–14° eccentricity. Following a variable delay period (800–1,200 ms), the center target shrank to a single pixel (0.3° × 0.3°) to signal the animal to make reaching movement to the target without breaking the eye fixation. This task was used to determine the preferred direction; that is, the direction associated with the maximum neuronal response of the cell was recorded (see *Recording procedures* below).

In the main task (Fig. 1, *A* and *B*), one "eye" target and one initial "hand" target were illuminated simultaneously (both 0.9° × 0.9°). These two targets could appear in one of five initial configurations: *Aligned*, *Eyes Right*, *Eyes Left*, *Hand Right*, and *Hand Left* (Fig. 1*A*). In each configuration, either the eye target or the initial hand position was at the center of the screen, directly in front of the animal. The other target (hand or eye) was at one of three possible positions (*P1–P3*): at the center of the screen or 7.5° to either side of the center, along an imaginary line that was perpendicular to the cell's preferred direction. For one animal, the eye target was red, and the initial hand target was green, and for the other animal, this was reversed. On *Aligned* trials (both targets at center), a blue target was used.

After the animal touched and fixated the initial hand and eye targets (450 ms), the peripheral target for a final reach (2.4° × 2.4°) appeared at one of eight possible target locations. Animals maintained the initial eye and hand position (within 4° and 5° of the center, respectively) for a variable delay period (900–1,300 ms; 50 ms steps) after the peripheral target onset. The initial eye and hand targets then shrank to a single pixel, cueing the animal to touch the peripheral target (within 5–6°) without moving the eyes from the eye target. Final reach targets *T1–T5* were spaced 7.5° apart along a line perpendicular to the preferred direction and 12–14° away from the center target (Fig. 1*A*). Target *T6* was directly opposite to the preferred direction. In 109 cells (87%), we also included targets *T7* and *T8*, orthogonal to the preferred direction. Targets *T6–T8* were presented only in the *Aligned* configuration, at 12–14° eccentricity to measure the null direction responses and to maintain a full range of potential reach directions. For most neurons, eight or nine repetitions of all 26 or 28 conditions [five targets (*T1–T5*) for each of the four noncentral initial configurations, plus six or eight targets (*T1–T6* or *T1–T8*) for the *Aligned* condition] were randomly interleaved for each limb.

The animals reached with the use of either the left or right forelimb in three alternating blocks (ABA design: contralateral block, ipsilateral block, contralateral control block), in which the unused hand was held off to one side of the target array throughout the entire block. A plastic panel was positioned so as to prevent the animals from reaching with the unused hand. Animals were visually monitored to ensure that they did not move the unused hand behind the panel in any systematic way.

When an error occurred (a failure to achieve or maintain fixation or touch at the initial targets throughout the delay period, an inaccurate movement to the target, or failure to maintain fixation during the reach), the trial was aborted, a multicolored square appeared briefly on the screen as an error signal, and a short (0.5- to 1.5-s) time-out ensued. Aborted trials were excluded from further analyses. Successful trials were rewarded with a drop of water or juice.

Recording procedures. We recorded neurons from two male monkeys. Extracellular recordings were made using glass-coated tungsten electrodes (Alpha Omega, Alpharetta, GA). Cells were recorded from the right hemisphere from *monkey G* and left hemisphere from *monkey S*.

Once a cell was isolated, we identified its approximate preferred direction using the preferred direction mapping task. For this, we used the reach direction that evoked the largest response in the 200-ms epoch following target onset, determined online. We then ran the main task, adjusting the target array for each neuron to obtain a tuning curve that fully spanned the response field. The variable starting hand and fixation positions (see above) allowed us to distinguish gaze-centered, hand-centered, and head-, body-, or world-centered responses. (Head-, body- and world-centered responses cannot be distinguished from one another in our paradigms.) We used the alternating limb blocks to ensure that isolation did not change over the course of the recording (see above). Cells that showed inconsistent modulations to the preferred direction target compared with the null direction target in the *Aligned* condition within the two contralateral-limb blocks were excluded ($P \leq 0.05$, two-tailed *t*-test). For the most critical analyses (noted in the text), we confirmed the results by applying a much more conservative criterion ($P \leq 0.40$) to rule out even subtle changes in isolation.

Data analysis. We considered responses in three main epochs: a 200-ms "visual" interval (50–250 ms from target onset time); a 700-ms delay period (850 ms before the time of the "Go" signal to 150 ms before the time of the Go signal); and a 250-ms peri-movement period (200 ms before to 50 ms after movement onset). (Similar results were obtained using slightly different time intervals and alignment points, e.g., a delay period from 150 to 850 ms after target onset or a visual period from 50 to 150 ms after target onset.) We focused on the delay-period interval. For each neuron and for each epoch, we calculated a limb specificity index

$$\frac{(Modulation_{contra\ hand}) - (Modulation_{ipsi\ hand})}{(Modulation_{contra\ hand}) + (Modulation_{ipsi\ hand})} \quad (1)$$

Modulation on contralateral- and ipsilateral-limb trials was measured under *Aligned* conditions. The modulation was computed as the

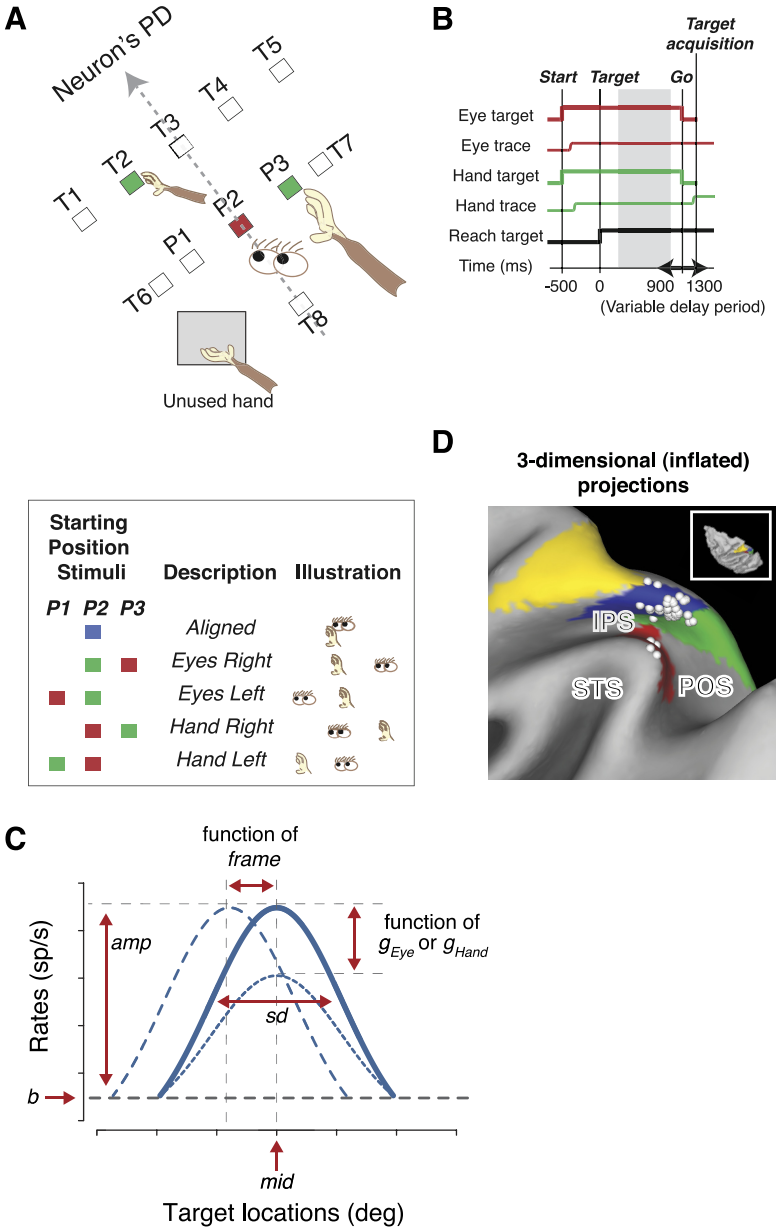

Fig. 1. Task design. *A*: behavioral task. Animals reached to 1 of 8 target locations from 1 of 5 configurations of initial eye and hand positions (box). *T1–T8* show potential target positions. *P1–P3* show potential positions for starting eye and hand positions. All conditions and targets were fully interleaved. PD, preferred direction. *B*: the temporal sequence of the behavioral task, aligned on reach target onset (time 0). The gray area represents the delay-period epoch. Start: onset of starting center eye and hand position targets; Target: reach target onset; Go: go signal. *C*: illustrated model parameters: baseline (*b*), amplitude (*amp*), middle of the tuning curve (*mid*), tuning width (*sd*), *frame*, and g_{Eye} and g_{Hand}; *frame* reflects the relative shift in the tuning curve with changes in initial eye or hand position, and g_{Eye} and g_{Hand} reflect changes in response amplitude with changes in initial eye and hand position, respectively. *D*: recording sites from *animal G* shown on a map of inflated cortex (http://brainmap.wustl.edu/caret). Cortical areas are color coded according to Lewis and Van Essen (2000a, b). Inset shows the dorsal view. Green, parieto-occipital (PO)/V6A (Galletti et al. 1999); blue, medial intraparietal area; yellow, dorsal area 5; red, lateral occipitoparietal area. IPS, intraparietal sulcus; STS, superior temporal sulcus; POS, PO sulcus.

difference between the mean of the firing rates for targets near the preferred direction (*T1–T5*) and the mean of the firing rates for targets in null directions (*T6–T8*). By taking this difference, we isolated the direction-specific effects of planning and executing a reach from differences in baseline firing, caused by, for example, potential postural differences between reaching with the ipsilateral vs. the contralateral limb. Since there are relatively few ipsilateral-limb cells in the PRR [11% in the current study and 16% in Chang et al. (2008)], we sometimes combined contralateral- and ipsilateral-limb cells together and analyzed them collectively as unilateral-limb cells.

We then fit the responses to each of the five main targets in each of the five starting conditions—a total of 25 values—to a seven-parameter nonlinear model (Chang et al. 2009; Chang and Snyder 2010). This model combines Gaussian tuning for the direction of the target with gain fields for the initial eye and hand positions

$$Firing\ rate = amp \times exp^{\frac{-(\theta - mid)^2}{2 \times sd^2}} \times (1 + E \times g_{Eye}) \times (1 + H \times g_{Hand}) + b. \quad (2)$$

We refer to *Eq. 2* as "the full model" in the text. The fit was performed using the nonlinear least squares (nls) function in the R statistics package (www.R-project.org), which determines the nls estimates of the parameters of a nonlinear model using the Gauss-Newton algorithm. The model inputs were firing rates, target eccentricity along the preferred direction (*ecc*; the perpendicular distance between the lines formed by *P1–P3* and *T1–T5* in Fig. 1*A*, measured in degrees of visual angle), target displacement in a direction orthogonal to the preferred direction (*T*; degrees of visual angle measured along the line connecting *T1* to *T5*), and the displacement of the initial eye (*E*) and hand target (*H*) from the center point (*P2*) in degrees of visual angle. The output parameters were the baseline firing rate (*b*) and peak amplitude of modulation (*amp*), both in spikes/s (sp/s); the center of the tuning curve, measured in degrees of visual angle from target *T3* (*mid*); SD (*sd*) of the Gaussian tuning curve in degrees of visual angle; the amplitudes of the eye position gain field (g_{Eye}) and the hand position gain field (g_{Hand}), both in fractional modulation/degree; and a unitless *frame* parameter, which captured the frame of reference for a given cell, with frames of 1 and 0 corresponding to

purely gaze-centered and purely hand-centered cells, respectively. It is worthwhile to note that the terms eye and hand in the present paper are defined with respect to the screen on which we measured eye and hand positions (i.e., fixation and pointing positions on screen coordinates). Therefore, one should be cautious when generalizing the interpretation to three dimensions. Figure 1*C* illustrates model parameters on a sample tuning curve.

The gaze-centered (*Eq. 3*), hand-centered (*Eq. 4*), and head-, body-, or world-centered models (*Eq. 5*) are each identical to the full model, except for their respective θ terms

$$where\ \theta = tan^{-1}\left(\frac{T - (frame \times E + (1 - frame) \times H)}{ecc}\right)$$

$$\theta = \tan^{-1}\left(\frac{T - E}{ecc}\right) \quad (3)$$

$$\theta = \tan^{-1}\left(\frac{T - H}{ecc}\right) \quad (4)$$

$$\theta = \tan^{-1}\left(\frac{T}{ecc}\right) \quad (5)$$

During the fitting procedure, parameters were constrained as follows: from −5 to 100 sp/s for *b*, from 0 to 300 sp/s for *amp*, −1.5 to 2.5 for *frame*, −0.15 to +0.15 (−15% to +15%) of modulation/degree for g_{Eye} and g_{Hand}, −45° to 45° for *mid*, and 15° to 60° for *sd*. These constraints were based on previously recorded data and by inspection of model fits. The particular features of the main task, including the number of targets and their spacing and eccentricity, were chosen with the help of a series of simulations. We simulated neuronal responses to a wide variety of task designs, using idealized cells whose characteristics (tuning width, response variability, etc.) were based on those of cells that we had recorded from the PRR in previous studies (Calton et al. 2002; Chang et al. 2008; Snyder et al. 1997). We used our idealized cells to generate artificial data using different task parameters and then analyzed those data to optimize the task design and to ensure that the fitting procedure was reliable.

Evaluation of model fits. We obtained spatial tuning curves from ~450 PRR neurons in two monkeys. We began recording in the main task for those neurons that were well isolated and spatially tuned (259 of all cells). We discontinued data collection prematurely in approximately one-half of these cells due to a change or loss in isolation. This resulted in a total of 125 spatially tuned neurons with three full blocks of alternating contralateral- and ipsilateral-limb blocks. Of the 125 cells, 123 passed our additional offline criterion for maintained isolation across blocks (similar responses within the two contralateral-limb blocks; see *Recording procedures* above for details). With the use of a much more conservative criterion for isolation (see *Recording procedures* above), 85 cells were accepted.

Model fits were judged based on how well the model accounted for firing rate. We took both the strength of the Gaussian tuning and the overall variance explained by the model into account. We combined these two factors into a single measure by multiplying variance explained (r^2) by the peak modulation of the Gaussian fit (sp/s) to obtain "spike-variance explained" (sp/s) (Chang et al. 2009; Chang and Snyder 2010). For the present study, we accepted neurons with a comparatively low criterion value of ≥2 sp/s spike-variance explained to increase the number of cells for comparing two different limbs. Out of 125 neurons, 71% ($n = 89$) and 62% ($n = 78$) of the recorded cells met this criterion during the delay period on contralateral- and ipsilateral-limb trials, respectively, and 53% ($n = 66$) met this criterion on both contralateral- and ipsilateral-limb trials. Acceptance based on different criterion values of spike-variance explained, variance explained alone, or χ^2 tests of the goodness of fit resulted in similar conclusions.

Location of the PRR. To guide the placement of our recording tracks and localize recording sites, we acquired high-resolution MRIs of monkeys' brains with an MR-lucent "phantom" in the recording chamber, using methods described elsewhere (Calton et al. 2002; Chang et al. 2008; Kalwani et al. 2009; Liu et al. 2010). Localization was accurate to within 1 mm, as determined by injecting and then visualizing MR-lucent manganese in the brain in several sessions.

The neurons we recorded straddle the boundary between the MIP and V6A (Luppino et al. 2005) in the PPC. The PRR was first localized as a region with a high proportion of neurons with strong visual responses and memory activity for visually presented targets, which is much stronger on impending reach trials than on impending saccade trials (Snyder et al. 1997). This region lies on the posterior portion of the medial bank of the intraparietal sulcus (IPS), close to the junction with the parieto-occipital sulcus, and often extends onto the lateral bank (see Fig. 1*D*) (Calton et al. 2002; Chang and Snyder 2010; Snyder et al. 1997). By combining our functional definition of the PRR with published histological tract-tracing data (Galletti et al. 1996; Lewis and Van Essen 2000a, b; Luppino et al. 2005; Matelli et al. 1998), it can be seen that the PRR primarily overlaps the anterior portion of V6A, the posterior portion of MIP, and a small part of lateral occipitoparietal area/caudal IPS (Fig. 1*D*). Whereas the borders of these anatomically defined areas vary somewhat from animal to animal and can vary greatly from study to study (Lewis and Van Essen 2000a, b), the PRR is well separated from lateral intraparietal area (LIP) and from the portion of the medial bank that lies directly across from LIP. In contrast to LIP, the PRR does not have a histologic or anatomic definition. However, it is worth noting that in neurophysiology studies, LIP is functionally defined, and this functional definition almost certainly does not overlap one to one with anatomical LIP. Therefore, the fact that the PRR is functionally defined rather than anatomically or histologically defined is not a unique circumstance.

To test for anatomical clustering across different limb specificities and reference frames, we used principle component analysis to identify the axis (within three-dimensional space) along which cells were most distributed. We then tested whether distinct cell populations (e.g., gaze- vs. hand-centered cells) were differentially distributed along that axis (Kolmogorov-Smirnov test).

RESULTS

Limb specificity. A total of 125 isolated units were recorded in the PRR from two animals (*monkey G*: 77; *monkey S*: 48 cells) performing delayed reaches with the contralateral and then with the ipsilateral hand (Fig. 1, *A* and *B*). Animals performed the task well, successfully completing 89% and 96% of the initiated trials (*monkeys G* and *S*, respectively), with median reach response latencies of 213 ± 42 ms and 261 ± 87 ms (±SD), respectively. The performances were comparable for the contralateral limb (93% correct; 226 ± 61 ms median response latency) and the ipsilateral limb (92%; 232 ± 69 ms). A subset of the contralateral-limb gain field and reference frame data was published previously (Chang et al. 2009; Chang and Snyder 2010); the ipsilateral-limb data have not been published.

Some PRR neurons represent target location when planning a reach with either limb, whereas others are more active when using just one or the other limb (Chang et al. 2008). We first replicated this finding in the current study. Figure 2*A* shows an example cell in the *Aligned* condition of the reaching task, where the starting eye and hand positions were aligned at the central position. Modulation was strong for reaching with either limb. The peak activity was 35.0 ± 5.8 sp/s (mean ± SE) on contralateral-limb trials and 44.7 ± 7.8 sp/s on ipsilat-

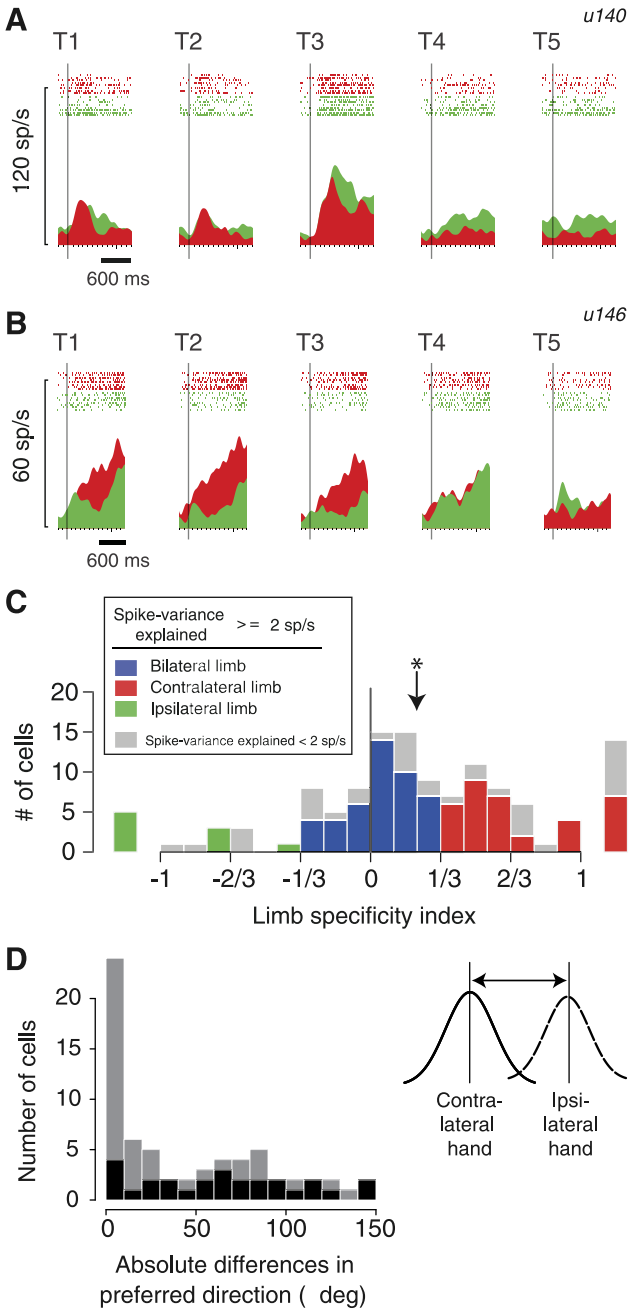

Fig. 2. Limb specificity. *A*: activity (peri-stimulus time histogram and rasters) of an example bilateral-limb cell (*u140*) in the *Aligned* condition. The vertical bars show the time of target onset. See Fig. 1*A* for the location of targets *T1–T5*. Responses with the ipsilateral limb in green; contralateral limb in red. *B*: activity of an example contralateral-limb cell (*u146*) in the *Aligned* condition. Same format as in *A*. sp/s, spikes/s. *C*: histogram of limb specificity indices (contrast ratios) of the entire PRR population during the delay period ($n = 125$). Cells with at least 2 sp/s spike-variance explained (cells with high variance explained; $n = 89$; see METHODS) are color coded according to the limb specificity index (see legend). Cells with <2 sp/s spike-variance explained are shown in gray. Cells with limb specificities >1 or −1 (e.g., 1.23) are shown separately in the margins. Arrow shows the median index, which was significantly greater than 0, indicating a contralateral-limb bias (*$P <$ 0.00001, Wilcoxon signed rank test). *D*: histogram of absolute preferred direction differences (Δ; in visual angles) for using the contralateral or ipsilateral limb. At the individual cell level, the preferred directions of 27 cells (41%) could be differentiated across the 2 hands (bootstrap test, $P < 0.05$; shown as dark bars).

eral-limb trials (not significantly different: $P = 0.41$, Wilcoxon signed rank test). In contrast, the cell in Fig. 2*B* showed a significant difference in activity between contralateral- and ipsilateral-reach plans (23.6 ± 2.6 vs. 14.1 ± 1.1 sp/s; significantly different: $P < 0.005$).

To quantify limb specificity across individual neurons, we computed the limb specificity index, a contrast ratio of the depth of modulation on contralateral- vs. ipsilateral-limb trials during the delay period (see METHODS; *Eq. 1*). The values range from −1 to +1, with positive numbers reflecting greater activity prior to contralateral-limb movements. The two example neurons have specificity ratios of −0.10 [nearly equal modulation (preferred minus null direction responses) and thus relatively limb-nonspecific; Fig. 2*A*], and 0.57 (over three times more modulation prior to reaches with the contralateral compared with the ipsilateral limb; Fig. 2*B*) and thus strongly limb-specific, respectively.

Figure 2*C* shows the population distribution of the limb specificity index for the delay period for all recorded cells ($n = 125$). Based on arbitrary criteria (ratios of 2:1 and 1:2 for the response magnitudes of contralateral:ipsilateral), 58 cells (46.4%) were classified as "bilateral-limb cells", 53 cells (42.4%) as "contralateral-limb cells", and only 14 cells (11.2%) as "ipsilateral-limb cells". (We will sometimes refer to contralateral- and ipsilateral-limb cells jointly as "unilateral-limb cells".) We also computed the index during the visual and peri-movement periods. Across the 125 cells, visual, delay, and peri-movement modulations were stronger for contralateral- compared with ipsilateral-limb movements, with median-limb specificities of 0.15, 0.22, and 0.15, respectively. In each epoch, the median was significantly greater than zero [contralaterally biased ($P < 0.005$, Wilcoxon signed rank test)]. Thus PRR cells, overall, showed a selectivity toward reach plans using the contralateral limb.

The preferred directions of PRR cells remain more or less unchanged between using the contralateral and ipsilateral hand (Chang et al. 2008). We replicated this finding in this new dataset, which has no overlap with the cells used in Chang et al. (2008), by computing each cell's preferred direction using the *mid* parameter (see METHODS). Although there are some cells with large differences in the preferred directions, the overall population showed minimal differences [Fig. 2*D*; difference of 25.7 ± 5.5° (median and SE), not significantly different from zero; $P = 0.13$, Wilcoxon signed rank test], and these preferred directions were significantly correlated across the two limbs ($\rho = 0.49$; $P < 0.00005$, Spearman's rank correlation). However, this tells us nothing about the frame of reference used during movements of the two different limbs.

Reference frames for contralateral vs. ipsilateral limb: individual neurons. Previously, we reported that reference frames for targets of contralateral-limb movements are idiosyncratic to each cell and range from gaze-centered to hand-centered and also include intermediate representations (Chang and Snyder 2010). It is unknown, however, whether and how these reference frames might change when the ipsilateral limb is used to reach. Here, we show two example neurons: one that maintained the same reference frame across the two limbs and another that did not.

Figure 3 shows the responses of a gaze-centered cell using either the contralateral or ipsilateral limb (the same neuron shown in Fig. 2*A*). This cell had a delay-period modulation of 28.04 and 29.72 sp/s on the first and third (contralateral) limb blocks. These values do not differ significantly from one

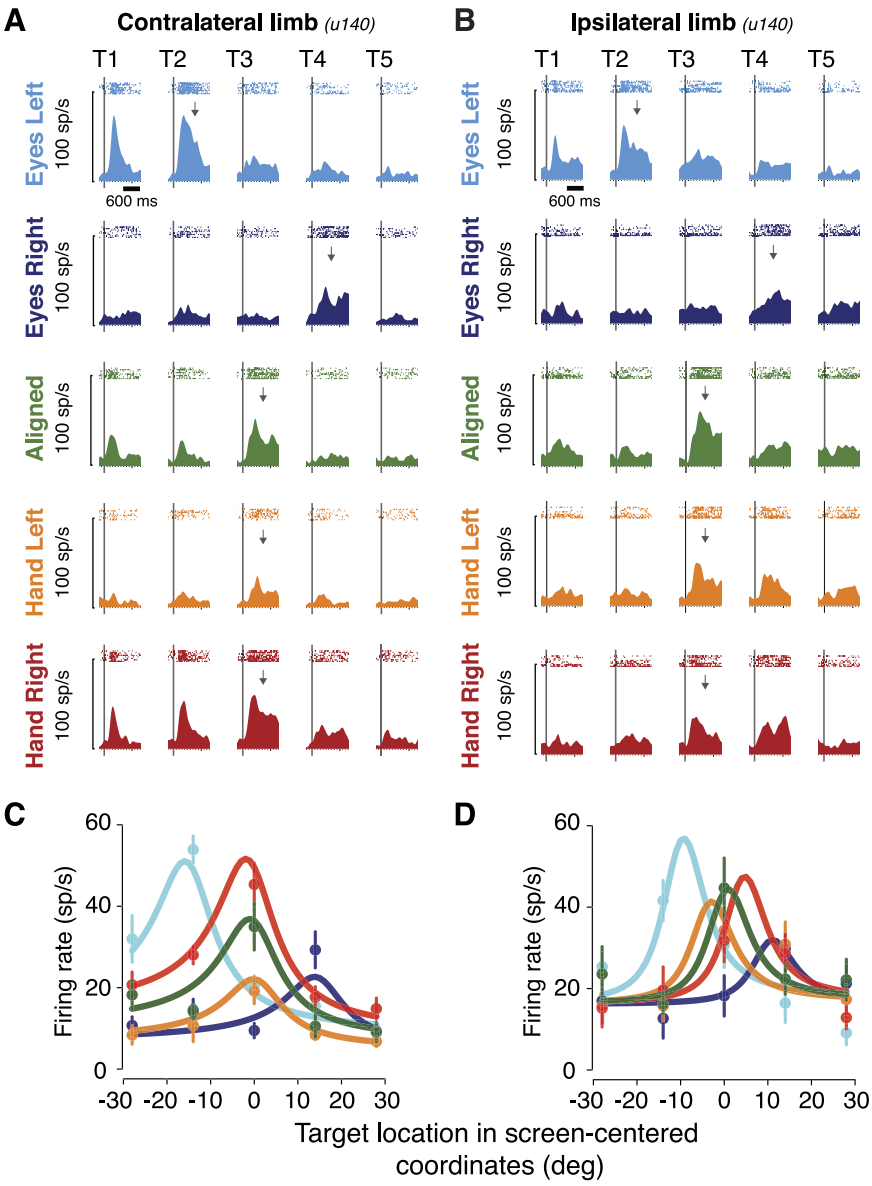

Fig. 3. An example bilateral-limb cell [the same cell shown in Fig. 2*A* (*u140*)], which encodes targets relative to the eyes (gaze-centered) on both contralateral- and ipsilateral-limb trials. *A*: peri-stimulus time histograms and rasters are color coded across 5 test conditions and 5 target locations (see Fig. 1) on contralateral-limb trials. Delay activity is shown with data aligned to the time of target onset (vertical lines). The peak location of the tuning curve fitted to each condition (see *C*) is indicated by arrows. *B*: peri-stimulus time histograms and rasters from ipsilateral-limb trials. Same format as in *A*. *C*: color-coded mean firing rates (circles), SE (bars), and fitted tuning curves vs. target locations on contralateral-limb trials are shown in screen-centered coordinates. The peak target positions of each condition's fitted tuning curve are indicated by arrows in *A*. *D*: color-coded mean firing rates, SE, and fitted tuning curves vs. target locations on ipsilateral-limb trials. Same format as in *C*.

another ($P = 0.91$, two-tailed *t*-test), evidence that isolation was maintained when the reaching limb was changed from contralateral (*block 1*) to ipsilateral (*block 2*) and back to contralateral (*block 3*). Consistent with the previous section, preferred direction did not change for the two limbs: with the eyes and hand aligned at the start of the trial, peak delay activity was evoked by the center target (*T3*) on both contralateral-limb (Fig. 3*A*) and ipsilateral-limb (Fig. 3*B*) trials. We now show that the frame of reference also did not change. Displacing the starting *Eye* position to the left or right caused peak delay-period activity to shift to the left or right (Fig. 3, *A* and *B*) when either limb was used. Peak activity remained at or very close to the center target (*T3*) when the starting position of the reaching hand was displaced to the left or right (Fig. 3, *A* and *B*), again, regardless of which hand was used. Tuning that shifts with eye position but not hand position is consistent with a gaze-centered representation and inconsistent with hand-, head-, body-, and world-centered representations. This gaze-centered representation did not depend on which limb was moved (limb-nonspecific reference frame), although the activity for this cell was highly specific for reaches compared with saccades (data not shown).

This neuron displayed eye and hand position gain fields on contralateral-limb trials. Responses were greater for *Eyes Left* compared with *Eyes Right* (leftward increasing eye position gain, 53.9 ± 3.3 vs. 29.3 ± 4.4 sp/s; $P < 0.001$, two sample *t*-test) and for *Hand Right* compared with *Hand Left* (rightward increasing hand position gain 19.1 ± 3.0 and 45.4 ± 5.2; $P < 0.001$). Despite the opposite polarity of the eye and hand gain fields, their magnitudes were similar ($P = 0.19$, two sample *t*-test). Surprisingly, on ipsilateral-limb trials, there was no hand position gain field and there was a trend toward an eye position gain field (41.61 ± 4.96 vs. 29.82 ± 3.76 sp/s; $P = 0.08$, two sample *t*-test).

We fitted the data from the ipsilateral- and the contralateral-limb blocks to a nonlinear model that takes into account both the frame of reference and any eye and hand position gain fields (see METHODS; *Eq 2*; Fig. 3, *C* and *D*). A parameter of the

model ("frame") identifies the location of the origin of each cell's frame of reference. A frame of 1 corresponds to an origin at the visual fixation point and therefore, describes a purely gaze-centered cell, whereas a frame of 0 corresponds to an origin at the starting hand position and therefore, describes a purely hand-centered cell. Fractional frames correspond to origins lying along a line connecting the point of fixation with the starting hand position (a line intersecting *P2* and *P3* in Fig. 1*A*). For example, a frame of 0.5 corresponds to an origin midway between the eye and hand.

The frame computed for the example cell on contralateral-limb trials was 1.06 (significantly different from 0, $P < 0.00001$; not significantly different from 1, $P = 0.76$, bootstrap test), consistent with the use of a gaze-centered frame of reference. The frame on ipsilateral-limb trials was 0.73 (significantly different from 0, $P < 0.00001$; not significantly different from 1, $P = 0.30$), again reflecting the use of a gaze-centered frame of reference. A stepwise regression analysis (F test) revealed that a purely gaze-centered model (frame parameter forced to equal 1; *Eq. 3*) fit the data just as well as the full model (*Eq. 2*) on both contralateral- and ipsilateral-limb trials (F test, $P > 0.3$ for both). The gaze-centered model captured 93% and 76% of the variance on contralateral- and ipsilateral-limb trials, respectively. A head-, body-, or world-centered model (no eye and hand position dependency; *Eq. 5*) did not fit the data as well as the gaze-centered model on either contralateral- or ipsilateral-limb trials [Bayesian information criterion (BIC) for comparing the fits of parametric models with a different number of parameters]. Therefore, this bilateral-limb cell represented target location in a gaze-centered frame, not a hand-centered reference frame, on both contralateral- and ipsilateral-limb trials, consistent with our hypothesis that cells use similar frames of reference during reaching with one limb or the other.

Figure 4 shows data from a cell that was much more active during contralateral- compared with ipsilateral-limb movements (the same neuron shown in Fig. 2*B*), whose frame of reference during contralateral reaches was hand-centered. Peak

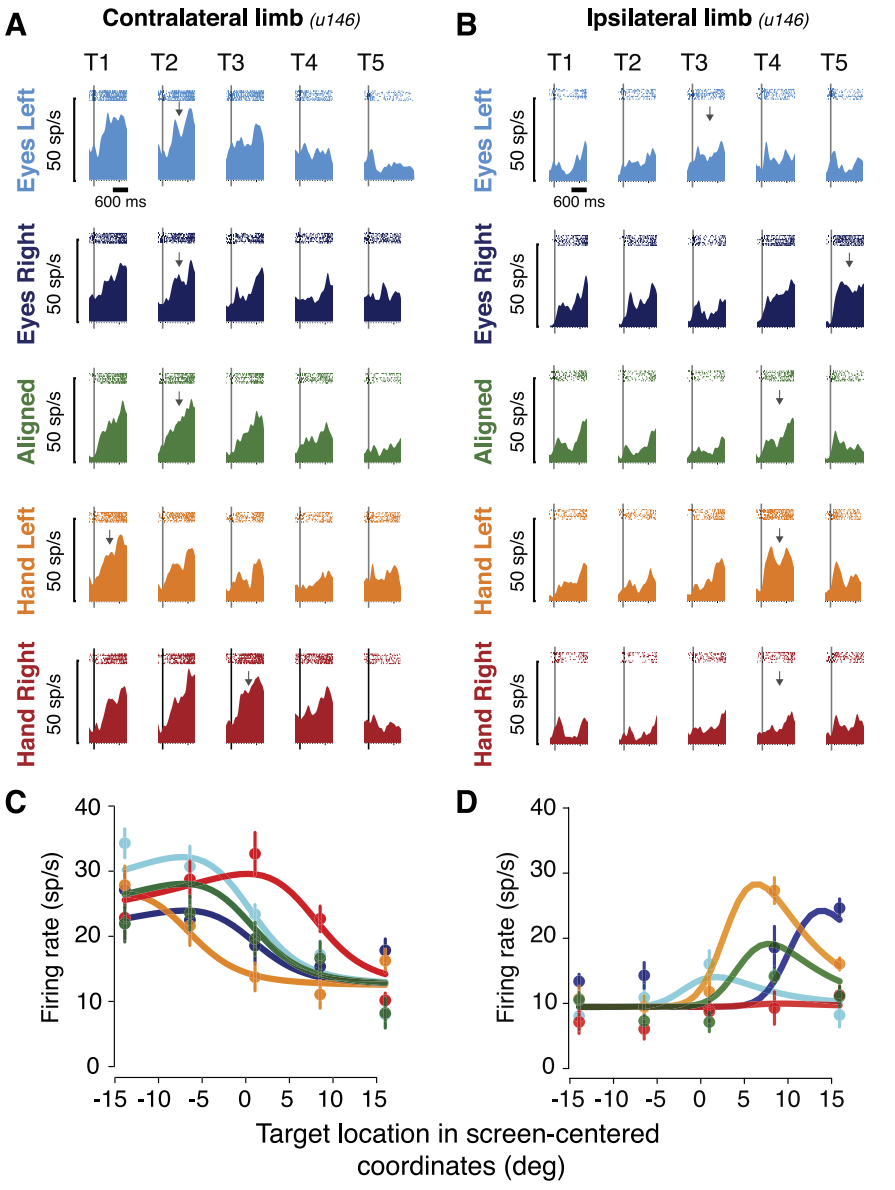

Fig. 4. An example contralateral-limb cell [the same cell shown in Fig. 2*B* (*u146*)], which encodes targets relative to the hand (hand-centered) only on contralateral-limb trials. *A*: peri-stimulus time histograms and rasters. *B*: peri-stimulus time histograms and rasters from ipsilateral-limb trials. Same format as in *A*. *C*: color-coded mean firing rates (circles), SE (bars), and fitted tuning curves vs. target locations on contralateral-limb trials. Format as in Fig. 3. *D*: color-coded mean firing rates, SE, and fitted tuning curves vs. target locations on ipsilateral-limb trials. Same format as in *C*.

delay activity under *Aligned*, *Eyes Left*, and *Eyes Right* conditions was evoked by targets *T1* and *T2*, but peak activity shifted to the left and right, respectively, under *Hand Left* and *Hand Right* conditions (Fig. 4*A*). Tuning that shifts with hand but not eye position is consistent with a hand-centered representation of target position. In contrast, on ipsilateral-limb trials, peak delay activity was evoked by target *T4* in the *Aligned* and *Hand Left* conditions (Fig. 4*B*). (In the *Hand Right* condition, the peak was not pronounced, due to flattening by the strong hand position gain field.) Peak activity shifted left and right, respectively, when starting eye position was shifted left or right (*Eyes Left* or *Eyes Right)*. This pattern is consistent with a gaze-centered representation.

These frames of reference were confirmed by modeling (Fig. 4, *C* and *D*). On contralateral-limb trials, the frame computed for this cell (*Eq. 2*) was 0.03, indicating that the reference-frame origin was close to the hand location (significantly different from 1, $P < 0.00001$; not significantly different from 0, $P = 0.58$, bootstrap test). A stepwise regression analysis revealed that a purely hand-centered model (frame parameter set exactly to 0; *Eq. 4*) fit the data as well as the full model (*F* test, $P = 0.89$), capturing 82% of the variance in firing rate, whereas a purely gaze-centered model did significantly worse than the full model ($P < 0.001$), capturing only 65% of the variance. A head-, body-, or world-centered model (*Eq. 5*) also did poorly (BIC). In contrast, on ipsilateral-limb trials, a purely gaze-centered model (*Eq. 3*) fit the data as well as the full model ($P = 0.44$), capturing 74% of the variance, whereas a purely hand-centered model (*Eq. 4*) did significantly worse ($P < 0.001$), capturing only 52% of the variance. Therefore, this unilateral-limb cell (much more active on contralateral-limb trials than on ipsilateral-limb trials) represented target location in a hand-centered frame on contralateral-limb trials but in a gaze-centered frame on ipsilateral-limb trials. This change in reference frame was not likely due to a change in cell isolation, since there was no significant change in delay-period modulation (preferred minus null direction activity in the *Aligned* condition) between the first and third (contralateral) limb blocks (8.93 sp/s vs. 12.78 sp/s; $P = 0.70$, two-tailed *t*-test).

Systematic relationship between reference frame and limb specificity. We next asked whether there is a systematic relationship between PRR reference frames and limb specificity. In Fig. 5, we contrast the reference frames of cells that are active when either limb is moved (bilateral-limb cells, 51 cells, 90 observations, blue data points) compared with cells that are primarily active for movements of just one limb (unilateral-limb cells, 42 cells, red data points; one observation/cell). Only data from model fits that met the 2 sp/s spike-variance explained criterion were considered. The bilateral-limb cell distribution is unimodal and heavily biased toward a gaze-centered frame of reference (median frame = 0.77 ± 0.09). The mode is close to gaze-centered (frame = 1), and there are few purely hand-centered cells (frame = 0). In contrast, the distribution for unilateral-limb cells (Fig. 5) appears to have two modes ($P < 0.06$, Hartigan's dip test). One mode is close to gaze-centered, like that of the bilateral-limb cells, but there is a second mode of hand-centered cells. The median for the unilateral-limb cells is only weakly biased toward a gaze-centered reference (0.61 ± 0.15 for all unilateral-limb cells; 0.66 ± 0.17 for contralateral-limb cells; and 0.46 ± 0.3 for ipsilateral-limb cells). The unilateral- and bilateral-limb distributions differ significantly, with more gaze-centered bias in the

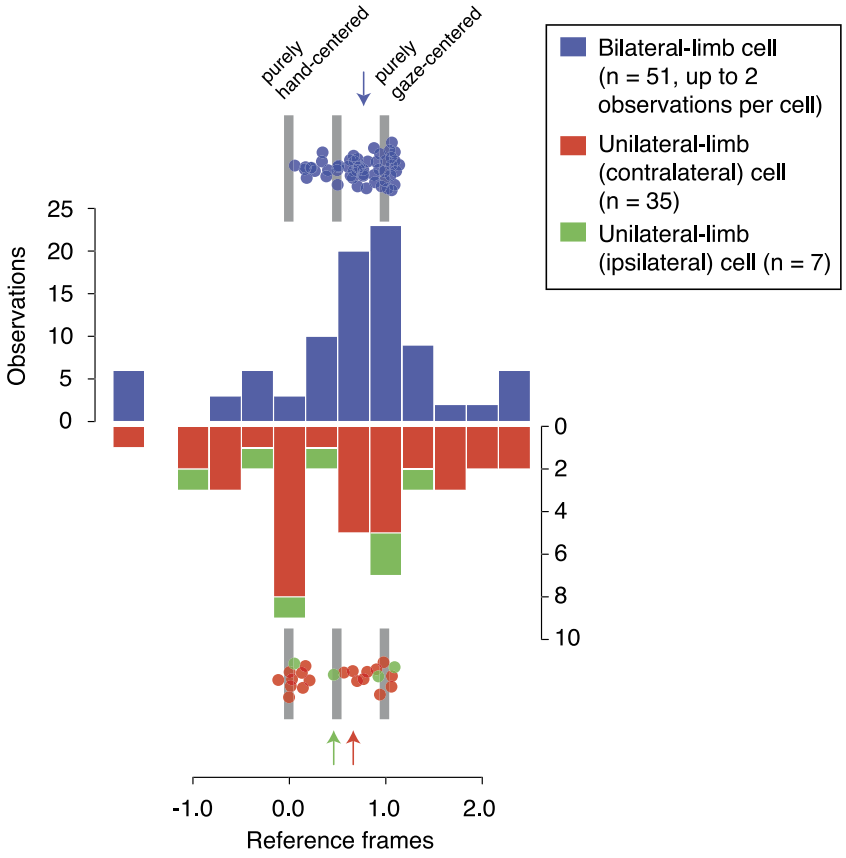

Fig. 5. Population relationship between reference frames and limb specificities. Distributions of reference frames (frame parameter of the model; *Eq. 2*) for bilateral-limb cells (both contralateral- and ipsilateral-limb blocks; $n = 51$; up to 2 observations/cell) and unilateral-limb cells (contralateral-limb cells—data from contralateral-limb blocks only, $n = 37$; ipsilateral-limb cells—data from ipsilateral-limb blocks only, $n = 7$; 1 observation/cell for unilateral-limb cells). Color-coded arrows indicate medians for each cell type. Points above and below the histograms show unbinned data points (only the in-bounds cells are shown on these data points). These individual data points are randomly jittered vertically to show overlapping data points.

bilateral-limb distribution ($P < 0.05$, one-tailed Kolmogorov-Smirnov test).

For Fig. 5, cells were divided into two categories based on whether they were at least two times as active during the planning of movements for one limb vs. the other. We also considered other classifications schemes and consistently found a bimodal distribution of unilateral-limb cells (data not shown). In Fig. 6, on the other hand, we show reference frame as a continuous function of limb specificity. For this analysis, we exclude out-of-bounds cells (reference frames outside of -0.15 to 1.15, $n = 32$; see below), cells with limb specificity index >1 or -1 ($n = 7$), and cells that were strongly ipsilateral-limb specific (limb specificity index -0.5; $n = 3$). We find that greater limb specificity is correlated with a more hand-centered frame of reference ($\rho = -0.41$, $P < 0.005$, Spearman's rank correlation; type II regression slope $= -1.69$, $P < 0.005$; $n = 47$). We observed similar results with our more conservative criterion for consistent isolation across task blocks (see METHODS; $\rho = -0.35$; $P < 0.05$). These results are consistent with the notion that bilateral-limb cells reflect a more sensory representation (gaze-centered and not limb specific), whereas unilateral-limb cells reflect a more motoric representation (hand-centered and limb-specific).

We did not observe evidence for different anatomical clusters with respect to limb specificities and reference frames in the PRR. Consistent with a previous report (Chang et al. 2008), the distributions of bilateral- and unilateral-limb cells were anatomically indistinguishable ($P = 0.74$, Kolmogorov-Smirnov test; see METHODS). Similarly, there was no significant distinction between the distributions of gaze-centered vs. hand-centered cells ($P = 0.65$) or between gaze-centered, bilateral-limb vs. hand-centered, unilateral-limb cells ($P = 0.60$).

PRR reference frames depend on which limb will be moved. At the population level, the distributions of reference frame types, quantified by the model parameter frame, were remarkably similar for reaches planned using either the contralateral or ipsilateral limb (Fig. 7, *A* and *B*). We examined all cells (both bilateral- and unilateral-limb cells), whose fit to the full model (*Eq. 2*) met our criterion of 2 sp/s spike-variance explained (see METHODS) when using one or the other limb.

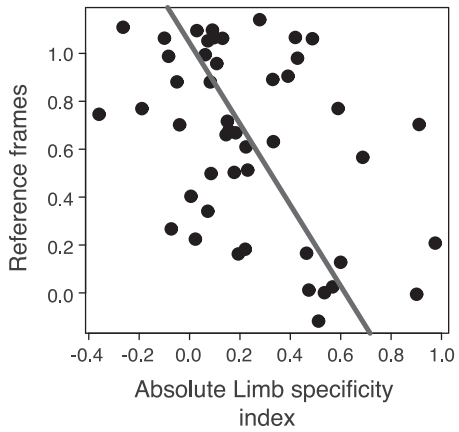

Fig. 6. Limb specificities are correlated with reference frames. Reference frame (frame parameter of the model; *Eq. 2*) is plotted as a function of the limb specificity. Cells with out-of-bounds reference frames ($n = 32$; see text), cells with limb specificity >1 or -1 ($n = 7$), and cells that strongly preferred the ipsilateral limb (limb specificity ratio -0.5; $n = 3$) were excluded from this analysis. Line through the data points represents type II linear regression.

Slightly more cells met the criterion on contralateral- compared with ipsilateral-limb trials [89 cells (71%) vs. 78 (62%)]. Among the 66 cells that met the criterion for both limbs, 8% more variance was explained, on average, on contralateral (65% explained)- vs. ipsilateral (57% explained)-limb trials. Consistent with our hypothesis that representations would be similar regardless of which hand was reaching, there was no significant difference between the two frame parameter medians [0.70 ± 0.09 (median ± SE) contralateral vs. 0.71 ± 0.11 ipsilateral], their overall distributions ($P = 0.87$, two-sample Kolmogorov-Smirnov test for the 66 cells that met the criterion with both limbs), or the percentage of gaze-centered (35% vs. 37%), hand-centered (19% vs. 19%), intermediate (17% vs. 18%), and unclassifiable cells (29% vs. 26%).

However, at the individual cell level, a different pattern emerged. For cells that were well fit by the model under both trial types, the model frame parameters on contralateral- and ipsilateral-limb trials were not significantly correlated with one another ($\rho = 0.20$; $P = 0.11$, Spearman's rank correlation; Fig. 7*C*). We observed a similar lack of correlation with our more conservative criterion for consistent isolation across task blocks (see METHODS; $\rho = 0.22$; $P = 0.18$). When the frame parameters were compared directly across the two trial types, 21% of the cells that fit both trial types showed significant shifts in reference frames (bootstrap test, $P < 0.05$). Thus at the population level, the reference frames used during contralateral- and ipsilateral-reach trials were remarkably similar, but at the individual cell level, the representations often differ.

From the population figures (Fig. 7, *A* and *B*), it is apparent that the reference frames of some cells were not gaze-centered, hand-centered, or intermediate between the two. We refer to cells with frames >1.15 or -0.15 as "out-of-bounds" cells, after Chang and Snyder (2010). Model fits for out-of-bounds cells do not explain as much variance as fits for in-bounds cells (mean spike-variance explained of 12.9 sp/s for out-of-bounds vs. 8.49 sp/s for in-bounds; $P < 0.05$, Wilcoxon rank sum test). Adding noise to in-bounds neurons can cause them to shift to be out-of-bounds neurons (Chang and Snyder 2010). These two findings suggest that out-of-bounds reference frames may be artifacts that arise when in-bounds cells are corrupted by noise. An alternative possibility is that out-of-bounds cells may encode spatial information in a way that is not well captured by our models (*Eqs. 2–5*). In any case, even if the out-of-bounds cells are excluded from Fig. 7*C*, the remaining 30 cells (Fig. 7*C*) still fail to show a significant correlation between the frame of reference used during reaches with each of the two limbs ($\rho = 0.29$; $P = 0.12$, Spearman's rank correlation).

It is possible that including noisy data results in poor or inappropriate fits and that these poor fits account for the apparent changes in reference frame between the two limbs. With poor fits, the parameters that the model settles on may be unreliable and may be strongly influenced by noise rather than the cell's responses. In such a scenario, the cell's reference frame may appear to change when reaching with one limb or the other, simply due to noise. If this were the explanation for why we see different reference frames for the two limbs, then we would expect that large shifts in reference frames would be observed in cells with poor model fits. We found this not to be the case. Figure 7*D* shows the magnitude of the difference in reference frames for reaches with the two limbs, plotted as a function of the lesser of the two model fits, that is, the lower of

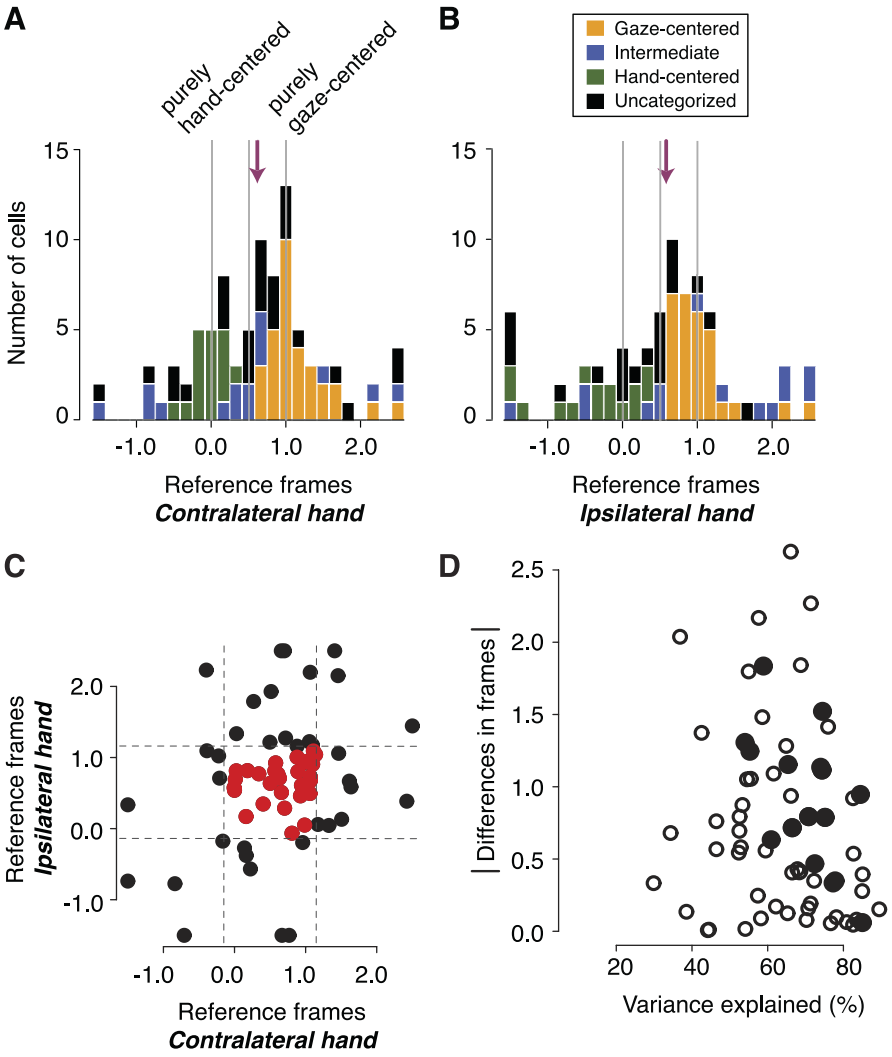

Fig. 7. Population reference frames and the differences of reference frames in individual neurons. *A*: the distribution of reference frames (frame parameter of the model; *Eq. 2*) from the delay period (*Eq. 2*) on contralateral-limb trials. Cells with at least 2 sp/s of spike-variance explained are shown ($n = 89$). Bars are color coded based on a stepwise regression (see text and box in *B*). Vertical lines represent values corresponding to pure hand-centered (frame = 0.0), pure gaze-centered (1.0), and exactly 1/2 between the 2 (0.5). Arrow, median. *B*: the distribution of frames from the delay period on ipsilateral-limb trials. Cells with at least 2 sp/s of spike-variance explained are shown ($n = 78$). Same format as in *A*. *C*: comparisons of reference frames (frames) across cells that fit both contralateral and ipsilateral limb with the spike-variance explained of at least 2 sp/s ($n = 66$). Dotted lines show the in-bounds vs. out-of-bounds reference frame boundaries. *D*: absolute shifts in reference frames (frames) across the 2 limbs as a function of model fits (variance explained). Plotted on the ordinate are poorer model fits between the 2 limbs (i.e., lower variance explained). Filled data points indicate the cells that significantly shifted frames across the 2 limbs by bootstrap test (21% of the cells that fit both trial types).

the two variance explained values. All but three of the cells that significantly shifted their frames (79%) had variance explained of 60% or greater (Fig. 7*D*), and the two variables are not correlated ($\rho = -0.20$; $P = 0.11$, Spearman's rank correlation). We found a similar pattern when we looked at the frame differences as a function of spike-variance explained ($\rho = -0.14$; $P = 0.26$, Spearman's rank correlation; data not shown). At the individual cell level, 43% of cells that significantly shifted frames showed spike-variance explained of 10 sp/s or greater. Therefore, poor fits do not fully account for apparent changes in reference frame between the two limbs.

PRR gain fields depend on which limb will be moved. When animals reach with the contralateral limb, PRR neurons have gain fields for both gaze and hand position. These gain fields have similar magnitudes but opposite signs, resulting in a single compound gain field that is proportional to the distance between ocular fixation and hand position (Chang et al. 2009). At the population level, the same was true during reaches with the ipsilateral limb. In the current data set, eye-to-hand position gain fields had median ratios of −0.84 and −0.94 during contralateral- and ipsilateral-limb reach trials, respectively. These values were not significantly different from the ideal ratio of −1 ($P = 0.15$ and 0.6, respectively, bootstrap test; $n = 66$ cells) and not significantly different from one another ($P = 0.5$, Wilcoxon sign rank test). However, at the individual cell level, we found clear differences between gain fields during ipsilateral- and contralateral-limb trials. Eye position gain fields on contralateral- and ipsilateral-limb trials were only weakly correlated (Fig. 8*A*; $r = 0.40$, $P < 0.001$, Pearson's correlation; type II regression slope = 0.99, $P < 0.001$; $n = 66$), and hand position gain fields were not correlated [across contralateral- and ipsilateral-limb trials (Fig. 8*B*; $r = 0.08$, $P = 0.54$; $n = 66$)]. We observed similar results with our more conservative criterion for consistent isolation across task blocks (see METHODS; $r = 0.08$, $P = 0.65$; $n = 40$). We also tested eye-hand compound gain fields between the two limbs. For this analysis, we fitted the data to a model where eye and hand position gain field terms are replaced by a single gain field for the signed distance between the eyes and the hand (see g_{Diff} in Chang et al. 2009). Compound eye-hand gain fields were also not correlated across the two limbs (Fig. 8*C*; $r = 0.16$, $P = 0.22$; $n = 60$). Thus like PRR reference frames, gain fields in the PRR for ipsilateral and contralateral reaches are grossly similar at the population level but very different at the single-cell level.

DISCUSSION

Neurons in the PRR encode information about the targets for visually guided reaching. We asked whether representations

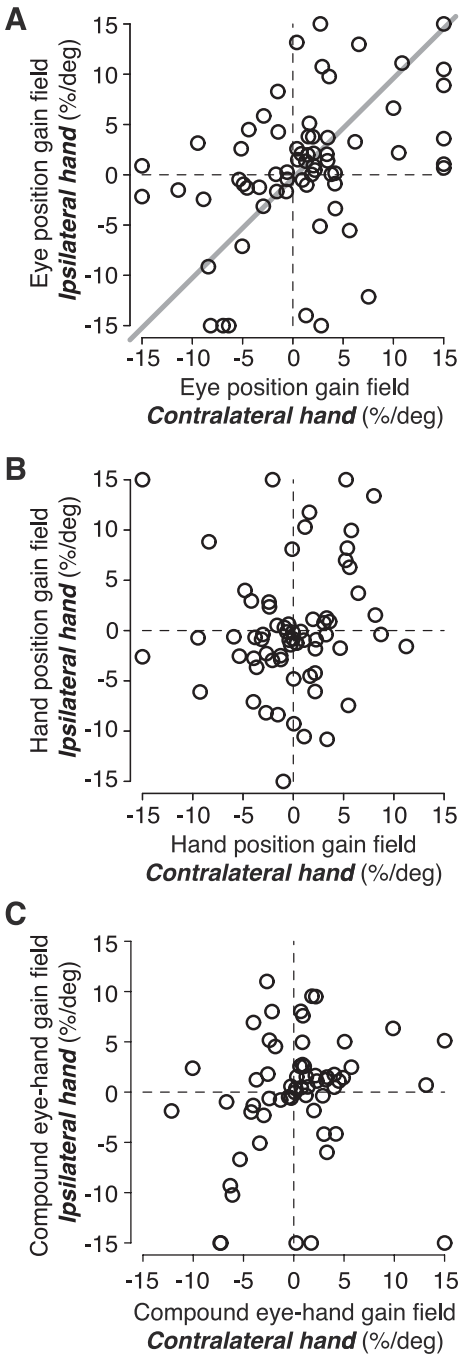

Fig. 8. Eye position gain fields, but not hand position gain fields, are correlated across using the contralateral and ipsilateral hand. *A*: eye position gain field magnitudes (%/deg) on contralateral- and ipsilateral-limb trials ($n = 66$). Line through the data points represents type II linear regression. *B*: hand position gain field magnitudes (%/deg) on contralateral- and ipsilateral-limb trials ($n = 66$). *C*: compound (eye–hand) gain field magnitudes (%/deg) on contralateral- and ipsialteral-limb trials ($n = 60$).

related to visually guided reaching depend on which limb is being used to reach. Previous studies have shown that preferred directions are preserved but that the magnitude of activation varies, in general, and is larger for contralateral-limb movements. We now show that frames of reference and gain fields in the PRR depend on which forelimb (ipsilateral or contralateral) will perform the reach (Figs. 7, *C* and *D*, and 8).

Not only do PRR reference frames depend on which arm moves, but we also found systematic differences in the reference frames between cells that are active for movements of either limb (bilateral-limb cells) and cells that are active for movements of just one limb (unilateral-limb cells). Bilateral-limb cells were strongly biased toward a gaze-centered frame of reference, whereas unilateral-limb cells were either gaze- or hand-centered (Fig. 5). Bilateral-limb cells that are hand-centered with respect to both limbs were extremely rare [e.g., only one bilateral-limb cell (2%) showed a reference frame within ±0.2 from the purely hand-centered reference frame; Fig. 5]. Interestingly, bilateral-limb cells that are hand-centered when one limb moved but gaze-centered (reference frame within ±0.2 from the purely gaze-centered frame) when the other limb moved were also rare (3% for one limb; 5% for the other), suggesting a systematic distribution of signals.

These results indicate that bilateral-limb cells reflect a more sensory representation (gaze-centered and not limb-specific) than unilateral-limb cells (hand-centered and limb-specific). The idea that gaze-centered, bilateral-limb cells are more sensory like is true in only a relative sense. These cells do not encode irrelevant stimuli and only weakly encode targets for upcoming saccadic eye movements and therefore, are quite different from true sensory cells (Chang et al. 2008; Snyder et al. 1997). This conclusion is supported further by the fact that the PRR encodes symbolically cued reach goals and anti-reach goals (Gail and Andersen 2006; Hwang and Andersen 2011). Similarly, the idea that hand-centered, limb-specific cells are more motor like is also only a relative truth. These cells encode movement endpoints, not muscle commands. More generally, many gaze-centered cells are limb-specific, and many limb-specific as well as bilateral cells have so-called intermediate reference frames; that is, they encode targets relative to locations somewhere between the point of fixation and the starting hand position (Duhamel et al. 1997). Thus the best description of the PRR is that it contains cells with mixtures of sensory-like and motor-like properties.

Not surprisingly, our model fits do not account for all of the variance in firing rate. Factors, which we did not measure, may account for some of this; for example, there might be postural changes in the body, limbs, and paw as the animal reaches for more eccentric, compared with more central, target locations. Another possibility is that modulations are not the idealized functions that we model them as; for example, the gain fields for eye and hand may be sigmoidal rather than linear. However, these issues do not substantially affect our principal findings.

Our data show clearly that PRR neurons behave differently, depending on with which limb the animal intends to reach. This was unexpected. The PPC has been thought to reflect an early stage of the sensorimotor transformation for reaching, especially compared with the PMd and M1 (Andersen et al. 1997; Kalaska et al. 1997). Although neurons in the PMd and M1 can be active for movements of either limb (Cisek et al. 2003; Kermadi et al. 1998, 2000), the amount of activity in any given cell depends strongly on which limb will move (Cisek et al. 2003; Donchin et al. 1998; Hoshi and Tanji 2000, 2002; Kermadi et al. 1998). This is consistent with a more motor-like organization. Based on the anatomical location of the PRR (lying between extrastriate visual and somatosensory cortices), its connectivity (Galletti et al. 1999; Gamberini et al. 2009;

Lewis and Van Essen 2000a, b; Luppino et al. 2005), and early reports of having a gaze-centered frame of reference (Batista et al. 1999; Buneo et al. 2002; Cohen and Andersen 2000), we expected that activity in the PRR would be more sensory like and would represent targets in ways that were relatively independent of the intended motor response. Instead, reference frames and gain fields depended on which limb was to be moved. This dependence suggests that the sensorimotor computations are limb-specific in the PRR.

Why should the representations of reach endpoints within individual cells differ, depending on which arm the animal plans on moving? The observation that a particular region carries a signal that is correlated with a particular behavioral output is generally taken as strong evidence that the region is involved in generating that behavior. This common, and potentially misleading, assumption suggests that the PRR has a causal role in both contralateral- and ipsilateral-limb movements. However, neural activations in and around the PRR in both humans and monkeys show a significant bias toward representing targets and somatosensation for the contralateral limb (Astafiev et al. 2003; Battaglini et al. 2002; Breveglieri et al. 2006; Chang et al. 2008; Connolly et al. 2003; Desmurget et al. 1999; Kermadi et al. 2000; Medendorp et al. 2003, 2005; Rice et al. 2007). Furthermore, in humans, it has been proposed that the medial IPS and the angular gyrus specify a reach vector relative to the contralateral hand (Vesia et al. 2008, 2010). Thus in both humans and monkeys, there is evidence for a contralaterally biased bilateral organization for reaching. In addition, under particular circumstances, delay-period activity in the PRR is correlated with contralateral- but not ipsilateral-reach reaction times (Chang et al. 2008; Snyder et al. 2006). Notably, in the current study, we find relatively few ipsilateral-specific, unilateral-limb neurons: the vast majority of unilateral-limb neurons was specific to representing target location for the contralateral limb. These findings support the possibility that the PRR controls only movements of the contralateral limb. If, in fact, the PRR is involved in controlling both limbs, then the information from each cell must be interpreted differently, depending on which limb will move. Such a conditional readout scheme is perfectly plausible when a single limb is being moved. However, often, there are plans to move both limbs to either the same or different targets. Under such circumstances, it is problematic to envision a readout of the PRR activity that is conditional on which hand will move.

If the PRR is concerned primarily with the contralateral limb, why are many cells active prior to an ipsilateral-limb movement? One possibility is that the decision to reach for a target (rather than to ignore it, merely attend to it, or look at it) is instantiated by spatial information regarding that target being routed to the PRR. A second decision, regarding which limb to use, may be instantiated by whether the bilateral-limb cell signals are propagated to the unilateral-limb cells. Thus the bilateral-limb cells would be activated on every trial, regardless of which limb was ultimately used for the reach. The unilateral-limb cells would then drive limb-specific cells in distal areas, such as the PMd (Hoshi and Tanji 2000, 2002). The idea that unilateral-limb cells may be closer to the motor output than bilateral-limb cells is supported by the finding that unilateral-limb cells are more likely to use a hand-centered reference frame than bilateral-limb cells (Figs. 5 and 6).

Another alternative is that bilateral- and unilateral-limb cells reflect parallel channels of information flow. Parallel information flow is supported by the fact that visual transient activity occurs simultaneously in the two cell types, not serially (Chang et al. 2008) (also true in the current data set, although the data are not shown). What might the purpose of such parallel channels be? Bilateral-limb cells might provide gaze-centered information for downstream computations, whereas unilateral-limb cells might provide hand-centered information. Alternatively, if the PRR is involved in bimanual coordination, then bilateral-limb cells, along with the few unilateral-limb cells that are tuned to the ipsilateral limb, could provide information about what the other limb is doing to facilitate coordination between the two limbs (Dean et al. 2011). Accumulating evidence from multiple visuomotor areas suggests that the neural mechanisms for bimanual coordination may be distinct from the neural mechanisms of controlling a single limb (Donchin et al. 1998; Kermadi et al. 2000; Tanji et al. 1988), although it remains unclear whether there are distinct anatomical clusters for coordinated limb movements in the PRR.

A third possibility is that when animals are instructed to prepare a movement with just one arm, they form "contingency" plans to make the movement with the other arm. These contingency plans might be weaker than the instructed plans. As a result, activity in bilateral-limb cells would generally be greater prior to movements of the contralateral limb, when the PRR actually codes the movement, and would be weaker prior to movements of the ipsilateral limb, when the PRR encodes only a contingency plan. However, since this explanation posits that in every case, a contralateral-limb arm movement is being encoded, it would predict identical reference frames and gain field modulations regardless of whether an ipsilateral- or contralateral-limb movement is instructed. We therefore prefer one of the two previous explanations.

Finally, it is important to keep in mind that our previous arguments notwithstanding, the PRR may in fact be involved in controlling both limbs. The strongest argument in favor of this possibility is that the overall distribution of reference frames is strikingly conserved when switching limbs (Fig. 7, *A* vs. *B*). This conservation at the population level over contralateral- and ipsilateral-limb movements suggests that similar spatial information is being coded under both circumstances. Perhaps the readout of that information is configured in such a way that the reference frame of the individual neurons does not matter, and all that matters is the overall distribution of those frames.

To summarize our findings, we found that individual PRR neurons encode reaches differently, depending on which limb will move. At the population level, the distribution of reference frames across cells is also conserved (Fig. 7, *A* vs. *B*). However, at the single cell level, cells that are active when either limb moves tend to be gaze-centered, whereas most hand-centered cells are active for only one limb (Figs. 5 and 6). Furthermore, the reference frame and gain field of individual cells clearly depend on which limb moves (Figs. 7*C* and 8), although the preferred directions are conserved (Fig. 2*D*).

ACKNOWLEDGMENTS

We thank D. Angelaki, S. Wise, A. Batista, and V. Rao for helpful discussions; G. DeAngelis for help with designing the experiment; J. D. Crawford and G. Blohm for interesting discussions and suggestions over the

years; T. Malone, J. Vytlacil, and J. Baker for MRI and localization; and E. Proctor and T. Shew for technical assistance.

Present address of S. W. C. Chang: Dept. of Neurobiology, Center for Cognitive Neuroscience, Duke Univ. School of Medicine, Durham, NC 27701.

GRANTS

This work was supported by National Eye Institute Grant R01 EY012135 and Vision Core Grant EY002687.

DISCLOSURES

No conflicts of interest, financial or otherwise, are declared by the author(s).

AUTHOR CONTRIBUTIONS

Author contributions: S.W.C.C. and L.H.S. conception and design of research; S.W.C.C. performed experiments; S.W.C.C. analyzed data; S.W.C.C. and L.H.S. interpreted results of experiments; S.W.C.C. prepared figures; S.W.C.C. and L.H.S. drafted manuscript; S.W.C.C. and L.H.S. edited and revised manuscript; S.W.C.C. and L.H.S. approved final version of manuscript.

REFERENCES

Andersen RA, Snyder LH, Bradley DC, Xing J. Multimodal representation of space in the posterior parietal cortex, and its use in planning movements. *Annu Rev Neurosci* 20: 303–330, 1997.

Astafiev SV, Shulman GL, Stanley CM, Snyder AZ, Van Essen DC, Corbetta M. Functional organization of human intraparietal, and frontal cortex for attending, looking, and pointing. *J Neurosci* 23: 4689–4699, 2003.

Avillac M, Deneve S, Olivier E, Pouget A, Duhamel JR. Reference frames for representing visual and tactile locations in parietal cortex. *Nat Neurosci* 8: 941–949, 2005.

Batista AP, Buneo CA, Snyder LH, Andersen RA. Reach plans in eye-centered coordinates. *Science* 285: 257–260, 1999.

Batista AP, Santhanam G, Yu BM, Ryu SI, Afshar A, Shenoy KV. Reference frames for reach planning in macaque dorsal premotor cortex. *J Neurophysiol* 98: 966–983, 2007.

Battaglia-Mayer A, Ferraina S, Genovesio A, Marconi B, Squatrito S, Molinari M, Lacquaniti F, Caminiti R. Eye-hand coordination during reaching. II. An analysis of the relationships between visuomanual signals in parietal cortex and parieto-frontal association projections. *Cereb Cortex* 11: 528–544, 2001.

Battaglini PP, Muzur A, Galletti C, Skrap M, Brovelli A, Fattori P. Effects of lesions to area V6A in monkeys. *Exp Brain Res* 144: 419–422, 2002.

Blohm G, Keith GP, Crawford JD. Decoding the cortical transformations for visually guided reaching in 3D space. *Cereb Cortex* 19: 1372–1393, 2009.

Breveglieri R, Galletti C, Gamberini M, Passarelli L, Fattori P. Somatosensory cells in area PEc of macaque posterior parietal cortex. *J Neurosci* 26: 3679–3684, 2006.

Buneo CA, Jarvis MR, Batista AP, Andersen RA. Direct visuomotor transformations for reaching. *Nature* 416: 632–636, 2002.

Burnod Y, Grandguillaume P, Otto I, Ferraina S, Johnson PB, Caminiti R. Visuomotor transformations underlying arm movements toward visual targets: a neural network model of cerebral cortical operations. *J Neurosci* 12: 1435–1453, 1992.

Calton JL, Dickinson AR, Snyder LH. Non-spatial, motor-specific activation in posterior parietal cortex. *Nat Neurosci* 5: 580–588, 2002.

Caminiti R, Johnson PB, Galli C, Ferraina S, Burnod Y. Making arm movements within different parts of space: the premotor and motor cortical representation of a coordinate system for reaching to visual targets. *J Neurosci* 11: 1182–1197, 1991.

Chang SW, Dickinson AR, Snyder LH. Limb-specific representation for reaching in the posterior parietal cortex. *J Neurosci* 28: 6128–6140, 2008.

Chang SW, Papadimitriou C, Snyder LH. Using a compound gain field to compute a reach plan. *Neuron* 64: 744–755, 2009.

Chang SW, Snyder LH. Idiosyncratic and systematic aspects of spatial representations in the macaque parietal cortex. *Proc Natl Acad Sci USA* 107: 7951–7956, 2010.

Cisek P, Crammond DJ, Kalaska JF. Neural activity in primary motor and dorsal premotor cortex in reaching tasks with the contralateral vs. ipsilateral arm. *J Neurophysiol* 89: 922–942, 2003.

Cohen YE, Andersen RA. Reaches to sounds encoded in an eye-centered reference frame. *Neuron* 27: 647–652, 2000.

Colby CL. Action-oriented spatial reference frames in cortex. *Neuron* 20: 15–24, 1998.

Connolly JD, Andersen RA, Goodale MA. FMRI evidence for a "parietal reach region" in the human brain. *Exp Brain Res* 153: 140–145, 2003.

Connor CE, Gallant JL, Preddie DC, Van Essen DC. Responses in area V4 depend on the spatial relationship between stimulus and attention. *J Neurophysiol* 75: 1306–1308, 1996.

Crawford JD, Medendorp WP, Marotta JJ. Spatial transformations for eye-hand coordination. *J Neurophysiol* 92: 10–19, 2004.

Dean HL, Marti D, Tsui E, Rinzel J, Pesaran B. Reaction time correlations during eye-hand coordination: behavior and modeling. *J Neurosci* 31: 2399–2412, 2011.

Desmurget M, Epstein CM, Turner RS, Prablanc C, Alexander GE, Grafton ST. Role of the posterior parietal cortex in updating reaching movements to a visual target. *Nat Neurosci* 2: 563–567, 1999.

Donchin O, Gribova A, Steinberg O, Bergman H, Vaadia E. Primary motor cortex is involved in bimanual coordination. *Nature* 395: 274–278, 1998.

Duhamel JR, Bremmer F, BenHamed S, Graf W. Spatial invariance of visual receptive fields in parietal cortex neurons. *Nature* 389: 845–848, 1997.

Fattori P, Gamberini M, Kutz DF, Galletti C. "Arm-reaching" neurons in the parietal area V6A of the macaque monkey. *Eur J Neurosci* 13: 2309–2313, 2001.

Fetsch CR, Wang S, Gu Y, Deangelis GC, Angelaki DE. Spatial reference frames of visual, vestibular, and multimodal heading signals in the dorsal subdivision of the medial superior temporal area. *J Neurosci* 27: 700–712, 2007.

Felleman DJ, Van Essen DC. Receptive field properties of neurons in area V3 of macaque monkey extrastriate cortex. *J Neurophysiol* 57: 889–920, 1987.

Flanders M, Helms Tillery SI, Soechting JF. Early stages in a sensorimotor transformation. *Behav Brain Sci* 15: 309–362, 1992.

Gail A, Andersen RA. Neural dynamics in monkey parietal reach region reflect context-specific sensorimotor transformations. *J Neurosci* 26: 9376–9384, 2006.

Galletti C, Fattori P, Battaglini PP, Shipp S, Zeki S. Functional demarcation of a border between areas V6 and V6A in the superior parietal gyrus of the macaque monkey. *Eur J Neurosci* 8: 30–52, 1996.

Galletti C, Fattori P, Kutz DF, Battaglini PP. Arm movement-related neurons in the visual area V6A of the macaque superior parietal lobule. *Eur J Neurosci* 9: 410–413, 1997.

Galletti C, Fattori P, Kutz DF, Gamberini M. Brain location and visual topography of cortical area V6A in the macaque monkey. *Eur J Neurosci* 11: 575–582, 1999.

Gamberini M, Passarelli L, Fattori P, Zucchelli M, Bakola S, Luppino G, Galletti C. Cortical connections of the visuomotor parietooccipital area V6Ad of the macaque monkey. *J Comp Neurol* 513: 622–642, 2009.

Goodale MA, Milner AD. Separate visual pathways for perception and action. *Trends Neurosci* 15: 20–25, 1992.

Hoshi E, Tanji J. Contrasting neuronal activity in the dorsal and ventral premotor areas during preparation to reach. *J Neurophysiol* 87: 1123–1128, 2002.

Hoshi E, Tanji J. Differential involvement of neurons in the dorsal and ventral premotor cortex during processing of visual signals for action planning. *J Neurophysiol* 95: 3596–3616, 2006.

Hoshi E, Tanji J. Integration of target and body-part information in the premotor cortex when planning action. *Nature* 408: 466–470, 2000.

Hwang EJ, Andersen RA. Spiking and LFP activity in PRR during symbolically instructed reaches. *J Neurophysiol* 107: 836–849, 2012.

Jay MF, Sparks DL. Sensorimotor integration in the primate superior colliculus. II. Coordinates of auditory signals. *J Neurophysiol* 57: 35–55, 1987.

Kakei S, Hoffman DS, Strick PL. Muscle and movement representations in the primary motor cortex. *Science* 285: 2136–2139, 1999.

Kalaska JF, Scott SH, Cisek P, Sergio LE. Cortical control of reaching movements. *Curr Opin Neurobiol* 7: 849–859, 1997.

Kalwani RM, Bloy L, Elliott MA, Gold JI. A method for localizing microelectrode trajectories in the macaque brain using MRI. *J Neurosci Methods* 176: 104–111, 2009.

Kermadi I, Liu Y, Rouiller EM. Do bimanual motor actions involve the dorsal premotor (PMd), cingulate (CMA) and posterior parietal (PPC) cortices? Comparison with primary and supplementary motor cortical areas. *Somatosens Mot Res* 17: 255–271, 2000.

Kermadi I, Liu Y, Tempini A, Calciati E, Rouiller EM. Neuronal activity in the primate supplementary motor area and the primary motor cortex in relation to spatio-temporal bimanual coordination. *Somatosens Mot Res* 15: 287–308, 1998.

Lewis JW, Van Essen DC. Corticocortical connections of visual, sensorimotor, and multimodal processing areas in the parietal lobe of the macaque monkey. *J Comp Neurol* 428: 112–137, 2000a.

Lewis JW, Van Essen DC. Mapping of architectonic subdivisions in the macaque monkey with emphasis on parieto-occipital cortex. *J Comp Neurol* 428: 79–111, 2000b.

Liu Y, Yttri EA, Snyder LH. Intention and attention: different functional roles for LIPd and LIPv. *Nat Neurosci* 13: 495–500, 2010.

Luppino G, Hamed SB, Gamberini M, Matelli M, Galletti C. Occipital (V6) and parietal (V6A) areas in the anterior wall of the parieto-occipital sulcus of the macaque: a cytoarchitectonic study. *Eur J Neurosci* 21: 3056–3076, 2005.

Marzocchi N, Breveglieri R, Galletti C, Fattori P. Reaching activity in parietal area V6A of macaque: eye influence on arm activity or retinocentric coding of reaching movements? *Eur J Neurosci* 27: 775–789, 2008.

Matelli M, Govoni P, Galletti C, Kutz DF, Luppino G. Superior area 6 afferents from the superior parietal lobule in the macaque monkey. *J Comp Neurol* 402: 327–352, 1998.

Maunsell JH Van Essen DC. Functional properties of neurons in middle temporal visual area of the macaque monkey. II. Binocular interactions and sensitivity to binocular disparity. *J Neurophysiol* 49: 1148–1167, 1983.

McGuire LM, Sabes PN. Heterogeneous representations in the superior parietal lobule are common across reaches to visual and proprioceptive targets. *J Neurosci* 31: 6661–6673, 2011.

McGuire LM, Sabes PN. Sensory transformations and the use of multiple reference frames for reach planning. *Nat Neurosci* 12: 1056–1061, 2009.

McIntyre J, Stratta F, Lacquaniti F. Viewer-centered frame of reference for pointing to memorized targets in three-dimensional space. *J Neurophysiol* 78: 1601–1618, 1997.

Medendorp WP, Goltz HC, Crawford JD, Vilis T. Integration of target and effector information in human posterior parietal cortex for the planning of action. *J Neurophysiol* 93: 954–962, 2005.

Medendorp WP, Goltz HC, Vilis T, Crawford JD. Gaze-centered updating of visual space in human parietal cortex. *J Neurosci* 23: 6209–6214, 2003.

Mullette-Gillman OA, Cohen YE, Groh JM. Eye-centered, head-centered, and complex coding of visual and auditory targets in the intraparietal sulcus. *J Neurophysiol* 94: 2331–2352, 2005.

Mullette-Gillman OA, Cohen YE, Groh JM. Motor-related signals in the intraparietal cortex encode locations in a hybrid, rather than eye-centered reference frame. *Cereb Cortex* 19: 1761–1775, 2009.

Pesaran B, Nelson MJ, Andersen RA. Dorsal premotor neurons encode the relative position of the hand, eye, and goal during reach planning. *Neuron* 51: 125–134, 2006.

Pouget A, Snyder LH. Computational approaches to sensorimotor transformations. *Nat Neurosci* 3, *Suppl*: 1192–1198, 2000.

Rice NJ, Tunik E, Cross ES, Grafton ST. On-line grasp control is mediated by the contralateral hemisphere. *Brain Res* 1175: 76–84, 2007.

Scott SH, Kalaska JF. Changes in motor cortex activity during reaching movements with similar hand paths but different arm postures. *J Neurophysiol* 73: 2563–2567, 1995.

Scott SH, Kalaska JF. Reaching movements with similar hand paths but different arm orientations. I. Activity of individual cells in motor cortex. *J Neurophysiol* 77: 826–852, 1997.

Snyder LH, Batista AP, Andersen RA. Coding of intention in the posterior parietal cortex. *Nature* 386: 167–170, 1997.

Snyder LH, Dickinson AR, Calton JL. Preparatory delay activity in the monkey parietal reach region predicts reach reaction times. *J Neurosci* 26: 10091–10099, 2006.

Stricanne B, Andersen RA, Mazzoni P. Eye-centered, head-centered, and intermediate coding of remembered sound locations in area LIP. *J Neurophysiol* 76: 2071–2076, 1996.

Tanji J, Okano K, Sato KC. Neuronal activity in cortical motor areas related to ipsilateral, contralateral, and bilateral digit movements of the monkey. *J Neurophysiol* 60: 325–343, 1988.

Vesia M, Prime SL, Yan X, Sergio LE, Crawford JD. Specificity of human parietal saccade and reach regions during transcranial magnetic stimulation. *J Neurosci* 30: 13053–13065, 2010.

Vesia M, Yan X, Henriques DY, Sergio LE, Crawford JD. Transcranial magnetic stimulation over human dorsal-lateral posterior parietal cortex disrupts integration of hand position signals into the reach plan. *J Neurophysiol* 100: 2005–2014, 2008.

Xing J, Andersen RA. Models of the posterior parietal cortex which perform multimodal integration and represent space in several coordinate frames. *J Cogn Neurosci* 12: 601–614, 2000.